American Mineralogist, Volume 69, pages 270–276, 1984

Lamellar structure of rhodonite and pyroxmangite intergrowths

NOBUYUKI AIKAWA

Department of Geosciences, Faculty of Science
Osaka City University, Sugimoto, 558 Osaka, Japan

Abstract

Reflections from X-ray and electron diffraction patterns of intergrowths of rhodonite and pyroxmangite are diffuse parallel to c*. Relatively sharp reflections correspond to ordered rhodonite or pyroxmangite. High resolution lattice fringe images show that units of rhodonite and pyroxmangite are intergrown as thin lamellae less than 300Å thick with (001) in common. Broadening of the powder X-ray lines and variation in the observed optical angle, $2V$, are explained on the basis of the lamellar structure of the two minerals.

Introduction

The paragenesis and intergrowth of rhodonite and pyroxmangite have been discussed by Burrell (1942), Momoi (1963, 1968), Suzaki (1963), Yoshimura (1967), Trommsdorff et al. (1970) and Ito (1972). Maresch and Mottana (1976) transformed synthetic pyroxmangite of composition $MnSiO_3$ to rhodonite at low temperature (about 400°C) and low pressure (about 3 kbar). They surmised that rhodonite will stably coexist with pyroxmangite provided that their chemical compositions are different. Peacor et al. (1978), Peters et al. (1978) and Winter et al. (1981) showed that the chemical compositions of coexisting rhodonite and pyroxmangite are different. Aikawa (1979) reported that intergrown rhodonite and pyroxmangite have a constant orientation relation; $\mathbf{a}_{rh}$ and $\mathbf{b}_{rh}$ are nearly parallel to $\mathbf{a}_{py}$ and $\mathbf{b}_{py}$, respectively, $\mathbf{c}_{rh}$ makes an angle of abour 4° with $\mathbf{c}_{py}$ on (110), and the chemical compositions of the two minerals are different (the subscript *rh* refers to rhodonite, *py* to pryoxmangite). Ried and Korekawa (1980) reported a new type of fault, called a chain periodicity fault which is approximately parallel to (001) and is due to irregularity in the periodicity along **c**, the direction of the silicate chain. For example, pyroxmangite was shown to have slabs of rhodonite one or more unit cells thick in the c-axis direction.

Momoi (1963) and Suzaki (1963) described two characteristics of rhodonite–pyroxmangite intergrowths: (1) broadening of reflections of the powder X-ray pattern, and (2) anomalous values of the optic angle $2V$. In order to understand these characteristics, this study of intergrowths of rhodonite and pyroxmangite from various localities has been carried out.

Specimens and experiments

Three samples used in this study are "rhodonite" from different localities. The fibrous rhodonite from the Sankei Mine, Hokkaido, which is a Au–Ag–Cu–Pb–Zn hydrothermal vein type deposit embedded in a green tuff complex covering Paleozoic sediments, occurs with quartz, rhodochrosite, pyrite, sphalerite and other metal sulfides (Suzaki, 1963). The filling temperatures of fluid inclusions in quartz associated with rhodonite range from 160 to 200°C. The "rhodonite" from the Ohedani Mine, Kyoto Prefecture and from the Kiyokawa Mine, Tokyo are both in strata-bound manganese ore deposits embedded in Paleozoic sediments. The Ohedani "rhodonite" occurs with quartz, rhodochrosite, tephroite and spessartine. The deposit has been regionally metamorphosed, and belongs to the epidote–actinolite zone of the greenshist facies (Hashimoto and Saito, 1970). The Kiyokawa "rhodonite" occurs as veinlets cutting rocks containing rhodochrosite, hausmannite, jacobsite, tephroite, bementite and spessartine. A petrologic study has not been carried out, but it is considered that the deposit has been regionally metamorphosed, perhaps under zeolite-facies conditions.

A preliminary survey of these specimens using powder X-ray diffraction methods resulted in their identification as a mixture of the two minerals as described by Momoi (1963) and Suzaki (1963). Fragments of the specimens were then studied by single-crystal X-ray methods. The cell dimensions were measured from **a**-, **b**- and **c**-axis precession photographs, and the profiles of diffuse reflections were measured using a densitometer. The chemical compositions of the fragments (remounted and polished after the single crystal X-ray experiments) were determined using a JXA-5A electron probe microanalyser with PET and RAP wavelength-dispersive crystal spectrometers. An accelerating potential of 15 kV and a sample current of 0.01 μA on MgO were the operating conditions. The beam current was digitized with counting times of 10 seconds on each of 5–10 areas of each grain analysed. Synthetic MgO, SiO_2, Al_2O_3, $CaSiO_3$, MnO, Fe_2O_3 and natural albite (Amelia, Virginia) were used as standards for all analysis. Analyses were carried out in the standard fashion with focused beam. Data sets were

0003–004X/84/0304–0270$02.00

reduced following the method of Bence and Albee (1968) using the α-factors given by Nakamura and Kushiro (1970). An electron microscope (Hitachi HU-12SE) operating at 100 kV and equipped with an energy dispersive X-ray analyzer was used for transmission electron microscopy. The specimen from Kiyokawa was prepared by ion milling a specimen from a thin section which was first oriented using single-crystal X-ray methods.

The diffraction pattern

Several precession patterns are shown in Figure 1. The shape of the diffuse reflections is columnar parallel to **c***. The profile of the diffuse reflections obtained using a densitometer parallel to **c*** is symmetrical around the intensity maxima. The positions of the intensity maxima correspond to those from ordered rhodonite or pyroxmangite. The orientational relation of the two minerals is in good agreement with that described previously (Aikawa, 1979).

Crystals from Kiyokawa give diffraction patterns corresponding to various phases, including: rh(s), rh(s) + py(d), rh(d) + py(d), rh(d) + py(s) and py(s), where (s) and (d) denote sharp and diffuse reflections, respectively. However, the specimens from Sankei give only two types of diffraction patterns; rh(s) + py(d) and rh(d) + py(s), and no single-phase crystal or sample of rh(s) + py(s) has been detected. The specimens from Ohedani always give sharp reflections of types rh(s), rh(s) + py(s) and py(s).

The electron diffraction patterns are similar to X-ray diffraction patterns. In Figure 2 are shown strong and sharp reflections corresponding to rhodonite and pyroxmangite connected by streaks parallel to **c***. However, intensity maxima which cannot be indexed with rhodonite or pyroxmangite cell parameters, are relatively sharp, and are superimposed on diffuse streaks, were often observed in electron diffraction patterns. The intervals between intensity maxima along diffuse streaks are not constant even in the same diffraction photograph, and also are different among diffraction photographs from different areas of the same crystal.

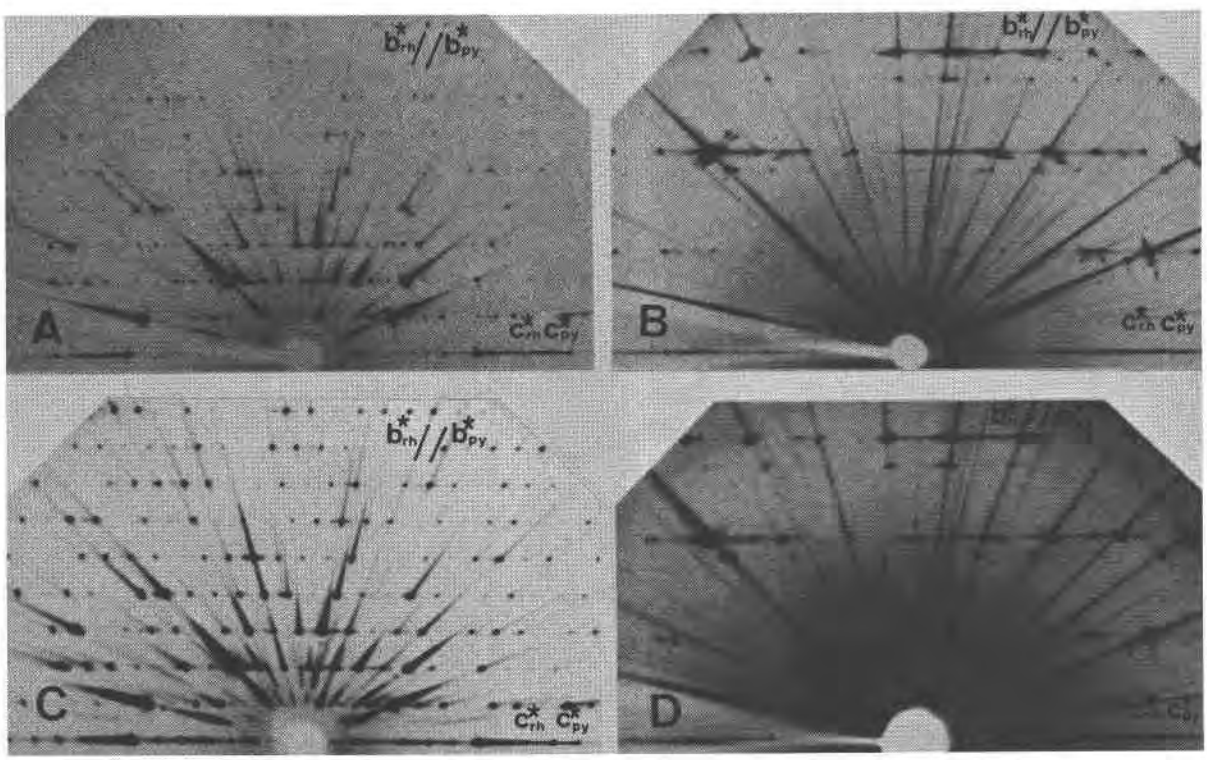

Fig. 1. Precession photographs of rhodonite and pyroxmangite intergrowths. (A) and (B). The 0*kl* net of the specimen, rh(d) + py(s), from Sankei. Two sets of reflections are apparent. One set of reflections is marked by the axes $\mathbf{b}^*_{py}$ and $\mathbf{c}^*_{py}$, and is due to pyroxmangite; the other set of reflections, marked by the axes $\mathbf{b}^*_{rh}$ and $\mathbf{c}^*_{rh}$, is due to rhodonite. The reflections from pyroxmangite are sharp, and those from rhodonite are diffuse. Photograph (A) was taken with Mo$K\alpha$ radiation, 120 hr. exposure. Photograph (B) was taken with Fe$K\alpha$ radiation, 150 hr. exposure. (C) and (D). The 0*kl* net of the specimen, rh(s) + py(d), from Kiyokawa. Two sets of reflections are apparent as in Figures 1A and 1B. The sharp reflections are due to rhodonite, and the diffuse reflections are due to pyroxmangite. Photograph (C) was taken with Mo$K\alpha$ radiation, 100 hr. exposure. Photograph (D) was taken with Fe$K\alpha$ radiation, 120 hr. exposure.

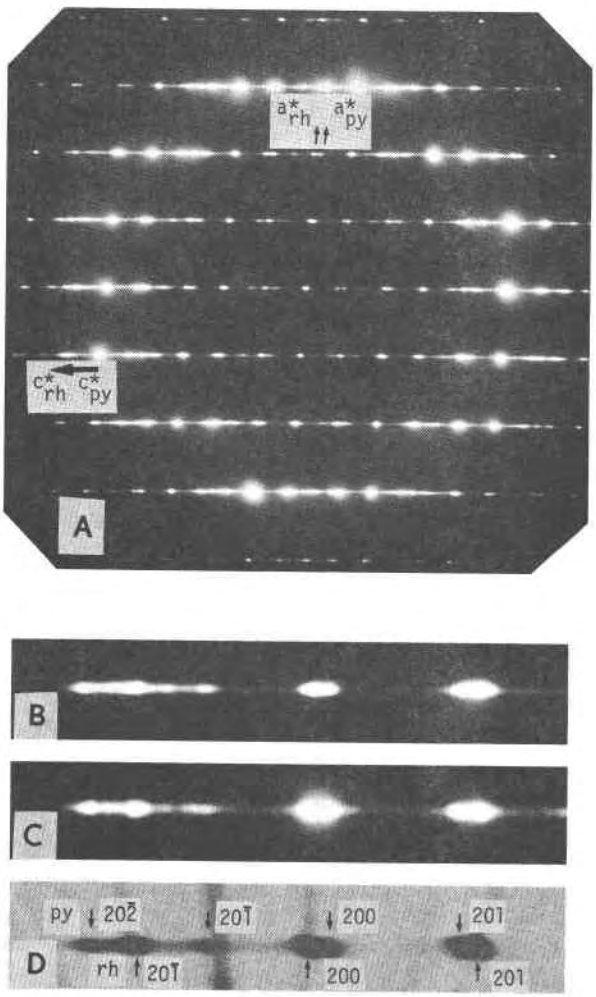

Fig. 2. Electron diffraction patterns and X-ray diffraction pattern of rhodonite and pyroxmangite intergrowths from Kiyokawa. (A) shows sharp reflections of rhodonite and pyroxmangite connected by strong streaks, in which intensity maxima are observable. (B) and (C) show 20*l* reflections of the electron diffraction photographs of two different areas of a crystal. (B) does not show well-defined subsidiary reflections, but (C) shows relatively sharp subsidiary reflections. (D) shows 20*l* reflections of the precession photograph of the crystal used in electron microscopy.

Chemical composition

The specimens consisting of two-phase intergrowths or of a single phase which were previously identified by single crystal X-ray methods have been examined using an electron probe microanalyser. The specimens were scanned parallel and perpendicular to the **c** axis in order to detect any chemical inhomogeneity, but none was found at the 1–2 μm resolution limit of the probe. The results are listed in Table 1.

The Ca content decreases in the order rh(s) + py(d), rh(d) + py(d) and rh(d) + py(s) in the Kiyokawa specimens. This result reconfirms the relation that rhodonite is more Ca-rich than pyroxmangite when the two minerals coexist (e.g., Aikawa, 1979; Winter et al., 1981; Brown et al., (1980). Pyroxmangite from the Kiyokawa Mine has less than 3 mole% $CaSiO_3$, and rhodonite has more than about 8 mole% $CaSiO_3$ (Aikawa, 1979). The compositional ranges of intergrowths of these two phases from the Kiyokawa Mine is thus between 3 and 8 mole% $CaSiO_3$. Twenty grains of the Sankei "rhodonite" were selected for analysis, but were not examined by single-crystal X-ray methods. The results are shown in Table 2. The Sankei specimens contain a larger amount of $CaSiO_3$. The composition of the Sankei "rhodonite" is divided into two ranges; one contains about 6–9 mole% $CaSiO_3$, the other about 13–17 mole% $CaSiO_3$. This is shown to relate to two types of diffraction patterns, rh(d) + py(s) and rh(s) + py(d), respectively. Pyroxmangite from the Sankei Mine has less than about 6 mole% $CaSiO_3$ and rhodonite has more than about 17 mole% $CaSiO_3$. Winter et al. (1981) reported compositions of rhodonite-pyroxmangite pairs from Bald Knob, North Carolina, together with previously published data. The results of this study, especially those of Sankei "rhodonite", do not agree with those reported by Winter et al. (1981). The difference in the composition ranges of the two intergrowth minerals from different localities may reflect different geological environments of formation of the specimens (Peters et al., 1977; Peacor et al., 1978; Brown et al., 1980; Winter et al., 1981).

Electron microscopy of rhodonite and pyroxmangite intergrowths

Rhodonite and pyroxmangite intergrowths show faults, planar and parallel to (001) as shown in Figure 3a, which are the same as those Ried and Korekawa (1980) observed in natural and synthetic pyroxenoids. There is no strain at these faults, and the contrast on both sides of a fault is quite uniform (Fig. 3a). The separation between these faults is about 50 to 300Å. Due to the faults, the diffraction patterns show streaks parallel to **c*** as shown in Figure 2. In order to elucidate the nature of the faults, high resolution lattice fringe images were obtained. The complex lattice fringe images (Fig. 3b) are similar to those of synthetic pyroxenoids as reported by Ried and Korekawa. These fringes are also parallel to (001) and there is no strain at the boundary. The widths of all fringes coincide with d_{001} of rhodonite and pyroxmangite, where d_{001} is nearly equal to $c \cdot \sin\alpha = 0.9c$ (Ried and Korekawa, 1980). There are homogeneous areas consisting of about 5–20 repeats of fringes of rhodonite or pyroxmangite and heterogeneous areas consisting of intergrowths of 1–3 fringes corresponding to rhodonite and pyroxmangite. However, fringes with widths corresponding to pyroxenoids with periodicities greater than 9 silicon tetrahedra were not observed. The complex and fine scale lamellar structure described in this study are explained by

Table 1. Analyses of rhodonites and pyroxmangites

Locality	Kiyokawa Mine					Sankei Mine
Sample	K-1	K-2	K-3*	K-4	K-5	S-2
	py	py(s)+rh(d)	py(d)+rh(d)	py(d)+rh(s)	rh**	py(d)+rh(s)
SiO_2	47.40	46.88	45.90, 47.75	48.43	47.45	47.34
Al_2O_3	0.05	0.07	0.08, 0.06	0.06	0.03	0.59
MgO	0.96	1.50	0.94, 1.04	0.70	0.78	0.87
FeO***	0.42	0.45	0.43, 0.49	0.38	1.03	0.31
MnO	51.37	50.69	50.09, 50.74	50.53	45.60	44.18
CaO	1.37	1.37	2.01, 1.94	2.77	6.36	7.11
Total	101.58	100.97	99.45,102.02	101.31	101.24	100.41
			Cations relative to 30 oxygens			
Si	10.04	9.98	9.96, 10.04	9.98	10.00	9.98
Al	0.01	0.02	0.02, 0.02	0.02	0.01	0.15
Mg	0.30	0.48	0.30, 0.33	0.22	0.24	0.27
Fe	0.08	0.08	0.08, 0.09	0.06	0.18	0.31
Mn	9.21	9.14	9.21, 9.04	9.10	8.14	8.06
Ca	0.31	0.31	0.47, 0.44	0.63	1.44	1.61

*Data of different points in same grain. **This occurs at boundary of bedded manganese ore body and massive chert. ***All assumed to be Fe^{2+}. (s)= sharp. (d)= diffuse.

"chain periodicity faults" which were first found in natural and synthetic pyroxenoids by Ried and Korekawa (1980); it can be completely explained by the occurrence of pyroxmangite (rhodonite) repeat units within rhodonite (pyroxmangite).

Discussion

The repeat distances of subsidiary reflections in electron diffraction patterns are not regular, differ from those reported by Ried and Korekawa, and do not show the

Table 2. Analyses of rhodonite and pyroxmangite intergrowths from the Sankei Mine

Sample	1	2	3	4	5	6	7	8	9	10
SiO_2	46.07	45.41	46.34	45.54	46.75	46.04	45.74	46.01	46.85	46.32
Al_2O_3	0.02	0.19	0.03	0.24	0.04	0.04	0.05	0.29	0.04	0.23
MgO	1.08	1.07	1.12	1.10	1.15	1.06	1.19	0.88	1.05	0.92
FeO*	0.28	0.20	0.28	0.28	0.29	0.25	0.26	0.28	0.26	0.28
MnO	49.66	49.74	49.97	49.85	49.68	49.67	49.37	49.08	49.04	48.64
CaO	2.81	2.86	2.93	2.99	3.09	3.17	3.29	3.51	3.54	3.79
Na_2O	0.03	0.05	0.06	0.03	0.00	0.00	0.02	0.00	0.00	0.03
Total	99.95	99.53	100.74	100.03	100.99	100.24	99.91	100.06	100.78	100.22
				Cations relative to 30 oxygens						
Si	9.94	9.86	9.92	9.84	9.95	9.91	9.88	9.90	9.98	9.93
Al	0.01	0.05	0.01	0.06	0.01	0.01	0.01	0.07	0.01	0.06
Mg	0.35	0.35	0.36	0.35	0.36	0.34	0.38	0.28	0.33	0.30
Fe	0.05	0.04	0.05	0.05	0.05	0.05	0.05	0.05	0.05	0.05
Ca	0.65	0.67	0.67	0.69	0.70	0.73	0.76	0.81	0.81	0.87
Na	0.01	0.02	0.03	0.01	0.00	0.00	0.01	0.00	0.00	0.01
Sample	11	12	13	14	15	16	17	18	19	20
SiO_2	46.31	46.38	45.88	46.13	56.01	46.32	45.51	45.15	46.01	46.55
Al_2O_3	0.27	0.29	0.30	0.37	0.64	0.52	0.16	0.18	0.15	0.22
MgO	0.90	0.96	0.78	0.79	0.82	0.84	0.81	0.88	0.86	0.80
FeO*	0.30	0.35	0.30	0.26	0.25	0.28	0.29	0.30	0.31	0.29
MnO	46.36	46.70	46.41	46.44	46.09	45.84	44.40	44.65	44.98	44.00
CaO	5.52	5.63	5.64	5.82	6.15	6.32	6.73	6.77	6.96	7.51
Na_2O	0.02	0.03	0.00	0.04	0.02	0.00	0.02	0.03	0.00	0.00
Total	99.69	100.34	99.31	99.85	99.99	100.13	97.92	97.95	99.28	99.37
				Cations relative to 30 oxygens						
Si	9.93	9.90	9.90	9.89	9.84	9.88	9.92	9.87	9.90	9.96
Al	0.07	0.07	0.08	0.09	0.16	0.13	0.04	0.05	0.04	0.06
Mg	0.29	0.31	0.25	0.25	0.26	0.27	0.26	0.29	0.28	0.26
Fe	0.05	0.06	0.05	0.05	0.05	0.05	0.05	0.05	0.06	0.05
Mn	8.42	8.44	8.48	8.43	8.35	8.28	8.20	8.26	8.20	7.97
Ca	1.27	1.29	1.30	1.34	1.41	1.45	1.57	1.59	1.61	1.72
Na_2O	0.01	0.01	0.00	0.02	0.01	0.00	0.01	0.01	0.00	0.00

*All assumed to be Fe^{2+}

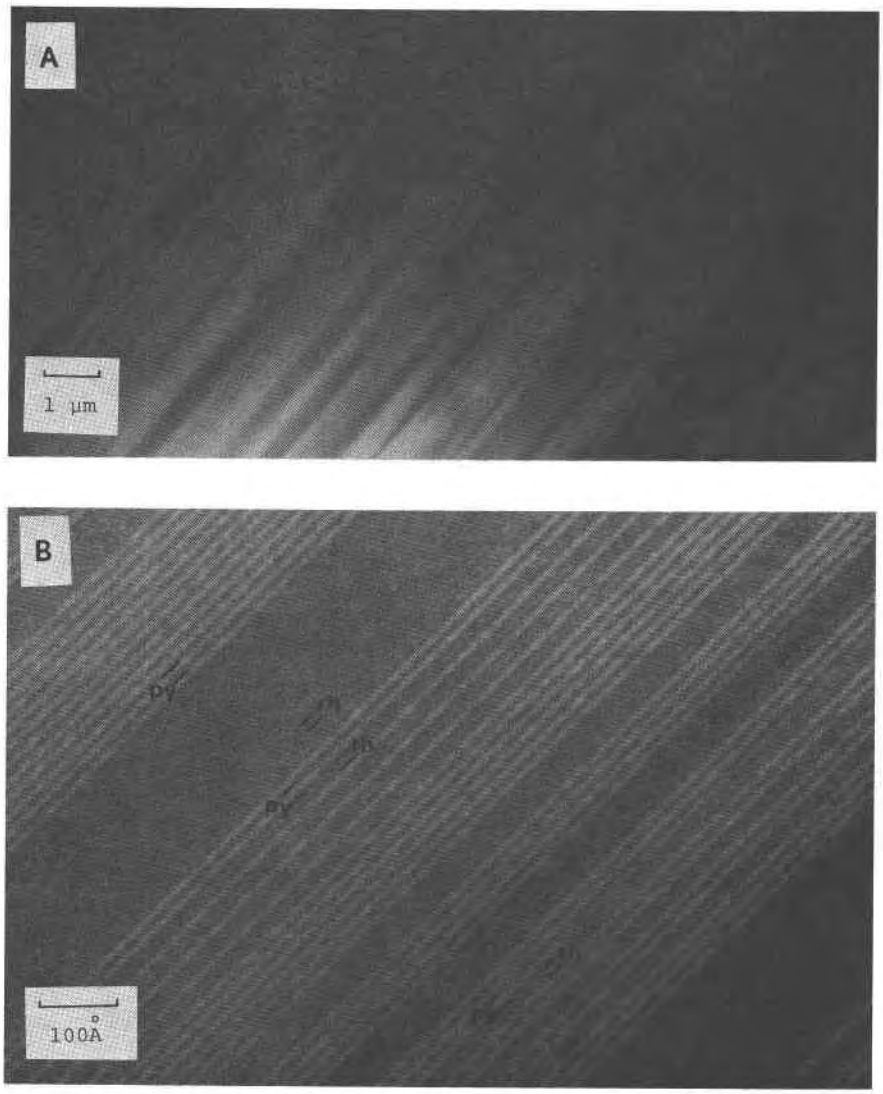

Fig. 3. Bright-field micrographs using 00*l* reflections of rhodonite and pyroxmangite intergrowths from Kiyokawa. (A) shows many faults with separations of 50 to 300Å. (B) Lattice fringe images. Widths of fringes correspond to d_{001} of rhodonite or pyroxmangite.

features such as doublets or triplets near reflections of rhodonite or pyroxmangite. Moreover, the diffraction patterns of different portions of a crystal are different from each other, as described previously. This shows that the areas giving diffraction patterns have different and irregular arrangements of chain periodicity faults. On the other hand, subsidiary reflections could not be observed in X-ray diffraction patterns. The X-ray diffraction pattern represents the average of the different electron diffraction patterns from various areas of a crystal, because the volume of crystal (about $0.5 \times 0.3 \times 0.2$ mm in this study) contributing to X-ray diffraction is very large compared with that (about $1 \times 1 \times 0.1$ μm) for electron diffraction. Therefore, subsidiary reflections could not be observed in X-ray diffraction patterns, and only the relatively sharp reflections corresponding to rhodonite and pyroxmangite connected with strong diffuse streaks could be observed, as can be seen in Figures 1 and 2d. The line broadening of the powder diffraction pattern (Fig. 4) can be explained by the same relations.

There is no strain at the faults. However, cell dimensions of rhodonite and pyroxmangite intergrowths as shown in Table 3 are somewhat different from those of single phase rhodonite or pyroxmangite; that is, b is longer and c is shorter than those of single phase rhodonite or pyroxmangite. This may be explained as simply being due to strain caused by coherency of the lamellar boundaries.

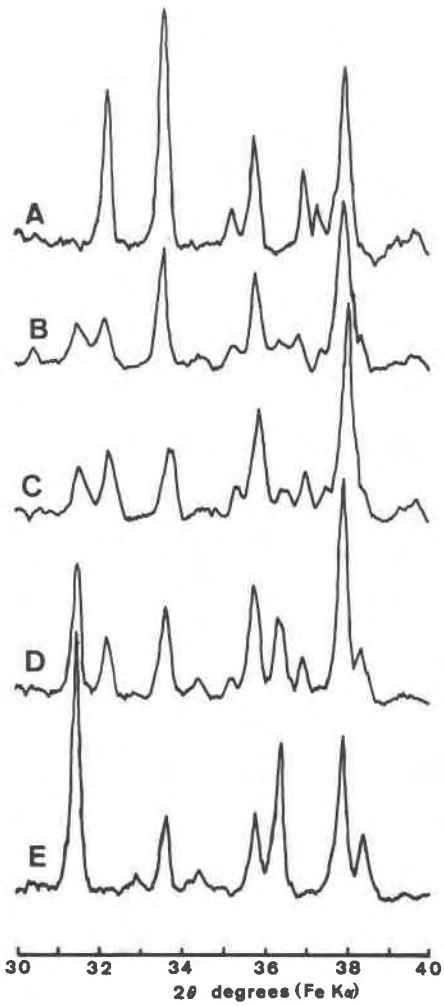

Fig. 4. Powder X-ray diffraction patterns between 14° and 18° and between 30° and 40° in $2\theta(\mathrm{Fe}K\alpha)$ of pyroxmangite (A), mixtures of rhodonite and pyroxmangite from different localities (B, C and D) and a single phase rhodonite (E). A: Ohedani. B: Sankei. C: Kiyokawa. D: Ohedani. E: Nodatamagawa, Iwate Prefecture.

Because most of the chemical and physical properties of rhodonite and pyroxmangite are very similar, it is difficult to distinguish between them by ordinary chemical and physical methods. However, the optic angle, $2V$, is very different; that of rhodonite is 63–87° and pyroxmangite 37–46° (Deer et al., 1978). Suzaki (1963) pointed out that specimens giving broad reflections in powder X-ray patterns show a wide variation in $2V$ ranging from 40 to 72°. The values of the specimen from the Kiyokawa Mine obtained using a universal stage have been confirmed to fall in the range of 48–70° (48, 52, 52, 64 and 70), although the number of measurements is only five. Homogeneously strained rhodonite and pyroxmangite as described in the last paragraph must give different optical angles compared with those of single-phase rhodonite and pyroxmangite. The intermediate values of $2V$ are thus explained by the lamellar structure. The thickness of lamellae is small in comparison with the wavelength used for the measurement of $2V$. If different domains of the crystal have different ratios of rhodonite and pyroxmangite as can be seen in Figure 3, then they must have different values of the average $2V$. The angle $2V$ may therefore vary over different portions of a crystal.

According to Ried and Korekawa (1980), their synthetic Fe-rhodonite and pyroxferroite have the same chemical composition. As described previously, Winter et al. (1981) and Aikawa (1979) showed that rhodonite is Ca-rich and pyroxmangite is Ca-poor when the two minerals coexist in nature. The present results of chemical compositions of rhodonite and pyroxmangite intergrowths using EPMA are in good agreement with those of coexisting natural pyroxenoids, although each of the two minerals could not be separately analyzed. In order to clarify the difference in chemical compositions of the two minerals existing in such fine-scale intergrowths, an analytical electron microscope was used, but it failed to elucidate the difference. This must be related to the resolution limit of the method, which is about 500Å.

Why did the complex natural rhodonite and pyroxmangite intergrowths form? Synthetic Fe-rhodonite and pyroxferroite intergrowths might be formed during crystal growth and natural rhodonite and pyroxmangite intergrowths might also be formed by the same process. However, it may also be necessary to consider some post-crystallization process such as exsolution. Pyroxenoids in nature always contain Ca, Fe, Mg, etc. substituted for Mn, so the experimental results obtained by Maresch and Mottana (1976) cannot be directly applied, and it is difficult to predict the change of P–T conditions of the transformation between multicomponent rhodonite and pyroxmangite. However, it is very interesting that rhodonite and pyroxmangite intergrowths in nature consist of separate parallel blocks of rhodonite and pyroxmangite and thus differ from synthetic Fe-pyroxenoids. Moreover, the conditions of formation of rhodonite and pyroxmangite intergrowths used in this study are quite different from those of the synthetic Fe-pyroxenoids; that is, the specimens in nature are considered to be formed under low temperature (200–400°C) and low pressure (less than approximately 3 kbar) conditions. Therefore, the natural rhodonite and pyroxmangite intergrowths may be formed by a process different from that of synthetic Fe-pyroxenoids.

Acknowledgments

The writer wishes to express his thanks to Prof. Y. Ohashi, University of Pennsylvania, and Dr. K. Koto, Osaka University for critical reading of the manuscript and many helpful suggestions. Dr. K. Nobugai, Osaka University, assisted with transmission electron microscopy. I should like to thank Prof. D. R. Peacor and Dr. E. J. Essene for improving the manuscript and

Table 3. Chemical compositions and cell dimensions

Locality	Sample		Composition (cations)	Cell dimension a(Å)	b(Å)	c(Å)	α(°)	β(°)	γ(°)
Kiyokawa mine	K-1	py(s)	$Ca_3Mg_3Mn_{93}Fe_1$	6.70	7.60	17.42	113.8	82.3	94.8
	K-2	py(s)	$Ca_3Mg_5Mn_{91}Fe_1$	6.70	7.63	17.35	113.8	82.4	94.8
		rh(d)		- - - - - not determined - - - - - - - - - -
	K-3	py(d)	$Ca_5Mg_3Mn_{91}Fe_1$	6.72	7.67	17.39	113.8	82.4	95.4
		rh(d)		6.70	7.62	12.19	111.0	84.9	94.4
	K-4	py(d)	$Ca_6Mg_2Mn_{91}Fe_1$	6.75	7.70	17.38	113.6	82.9	95.5
		rh(s)		6.71	7.64	12.20	111.3	85.1	94.4
	K-5	rh(s)	$Ca_{14}Mg_2Mn_{82}Fe_2$	6.73	7.68	12.25	111.5	85.0	94.4
Sankei mine	S-1	py(s)	not determined	6,75	7.65	17.37	114.1	82.6	94.3
		rh(d)		6.72	7.65	12.15	110.6	85.2	93.6
	S-2	py(d)	$Ca_{16}Mg_3Mn_{80}Fe_1$	6.74	7.71	17.36	113.1	82.7	94.8
		rh(s)		6.72	7.67	12.23	111.3	85.2	94.2

The interaxial angles are accurate to about 5 minutes, and the cell edges to approximately 0.2 to 0.3% with corrections made for film shrinkage.

for helpful advice. A part of the cost of this work was defrayed by a research grant from the Japanese Ministry of Education.

References

Aikawa, N. (1979) Oriented intergrowth of rhodonite and pyroxmangite and their transformation mechanism. Mineralogical Journal, 9, 255–269.

Bence, A. E. and Albee, A. L. (1968) Empirical correction factors for the electron microanalysis of silicate and oxide. Journal of Petrology, 76, 382–403.

Brown, P. E., Essene, E. J. and Peacor, D. R. (1980) Phase relations inferred from field data for Mn pyroxnes and pyroxnoids. Contributions to Mineralogy and Petrology, 74, 417–425.

Burrell, H. C. (1942) A statistical and laboratory investigation of ore types at Broken Hill, Australia. Harvard University Ph.D. Thesis (not seen; extracted from Deer et al., 1978).

Deer, W. A., Howie, R. A. and Zussman, J. (1978) Rock-Forming Minerals. Vol. 2A, John Wiley and Sons Inc., New York.

Hashimoto, M. and Saito, Y. (1970) Metamorphism of Paleozoic greenstones of Tamba plateau, Kyoto Prefecture. Journal of the Geological Society of Japan, 76, 1–6.

Ito, J. (1972) Rhodonite-pyroxmangite peritectic along the join $MnSiO_3$–$MgSiO_3$ in air. American Mineralogist, 57, 865–876.

Maresch, W. V. and Mottana, A. (1976) The pyroxmangite–rhodonite transformation for the $MnSiO_3$ composition. Contributions to Mineralogy and Petrology, 55, 69–79.

Momoi, H. (1963) Some problems on pyroxmangite. Journal of the Mining and Metallurgical Institute of Japan, 79, 836–837 (in Japanese).

Momoi, H. (1968) Some manganese pyroxenoids. Journal of the Mineralogical Society of Japan, 8, Special Issue 2, 1–6 (in Japanese).

Nakamura, Y. and Kushiro, I. (1970) Compositional relations of coexisting orthopyroxene, pigeonite and augite in a tholeiitic andesite from Hakone Volcano. Contributions to Mineralogy and Petrology, 26, 265–275.

Peacor, D. R., Essene, E. J., Brown, P. E. and Winter, G. A. (1978) The crystal chemistry and petrogenesis of a magnesian rhodonite. American Mineralogist, 63, 1137–1142.

Peters, Tj., Trommsdorff, V. and Sommerrauer, J. (1978) Manganese pyroxenoids and carbonates: Critical phase relations in metamorphic assembleges from the Alps. Contributions to Mineralogy and Petrology, 66, 383–388.

Ried, H. and Korekawa, M. (1980) Transmission electron mineralogy of synthetic and natural Fünferketten and Siebenerketten pyroxenoids. Physics and Chemistry of Minerals, 5, 351–365.

Suzaki, Y. (1963) Pyroxmangite, rhodonite and bustamite series minerals. Geoscience Magazine, 14, 72–87 (in Japanese with English abstract).

Trommsdorff, V., Schwander, H. and Peters, Tj. (1970) Manganosilicate der alpinen Metamorphose in Radiolariten des Julier-Bernina-Gebietes. Schweizersche Mineralogische und Petrologische Mitteilungen, 50, 539–554.

Winter, G. A., Essene, E. J. and Peacor, D. R. (1981) Carbonates and pyroxenoids from the manganese deposit near Bald Knob, North Carolina. American Mineralogist, 66, 278–289.

Yoshimura, T. (1967) Supplement to "Manganese ore deposits of Japan". Science Reports, Department of Geology, Kyushu University, 9 (Special Issue), 245–270 (in Japanese).

Manuscript received, June 30, 1981;
accepted for publication, August 30, 1983.